Thermally activated magnetization reversal in exchange-biased $[Pt/Co]_3/Pt/IrMn$ multilayers

Maciej Czapkiewicz,[1,*] Tomasz Stobiecki,[1] and Sebastiaan van Dijken[2,†]
[1]*Department of Electronics, AGH University of Science and Technology, 30-059 Kraków, Poland*
[2]*CRANN and School of Physics, Trinity College, Dublin 2, Ireland*
(Received 23 January 2007; revised manuscript received 11 May 2007; published 15 January 2008)

We report on the magnetization reversal in exchange-biased $[Pt/Co]_3/t$ Pt/IrMn multilayers with different Pt insertion layer thicknesses ($0 \leq t \leq 1.2$ nm). For $t=0$ nm and $t=0.2-0.8$ nm, magnetization reversal is asymmetric and proceeds by domain nucleation followed by a fast domain wall motion. For $t=0.1$ nm, domain nucleation is predominant. We interpret these results within a model for thermally activated reversal where a dispersion of the activation energy barrier is specifically taken into account. From magnetization relaxation curves, we are able to measure the barrier dispersion and identify the physical origin of different reversal effects: whereas reversal asymmetry is mostly due to local fluctuations of the anisotropy axis and exchange bias direction, the nucleation of a large number of inverse domains is caused by lateral variations of the interface exchange coupling energy. Moreover, we show that an improved perpendicular spin alignment in the outermost Co film maximizes the exchange coupling energy for a Pt insertion layer of 0.1 nm.

DOI: 10.1103/PhysRevB.77.024416 PACS number(s): 75.60.Jk, 75.30.Gw, 75.60.Ej, 75.70.Kw

I. INTRODUCTION

Exchange interactions between a ferromagnetic (FM) and an adjacent antiferromagnetic (AFM) material can lead to unidirectional exchange anisotropy. This phenomenon, which was originally discovered by Meikeljohn and Bean,[1] is characterized by a shift of the hysteresis curve, generally called exchange bias, and enhanced coercivity. For practical applications, exchange-biased bilayers of thin FM and AFM films have intensively been studied and are now an integral part of magnetic field sensors, computer read heads, and magnetic random access memories. In all these devices, the magnetic moment and exchange bias direction are aligned parallel to the film plane. More recently, exchange bias effects have been studied in systems exhibiting perpendicular magnetic anisotropy. Among them are $[Pd/Co]_n$/AFM and $[Pt/Co]_n$/AFM multilayers, where the AFM layer is either CoO,[2–5] FeMn,[6–14] IrMn,[15–21] or Ising-type AFM compounds such as FeF_2 and $FeCl_2$.[22,23] Perpendicular exchange bias effects have also been measured on Ni films sandwiched between a Cu(001) seed layer and an AFM.[24,25] While some of the properties of these structures, for instance, the evolution of the exchange bias field with FM[17,21,25] and AFM[6,18] layer thicknesses, resemble those of in-plane systems, others are more specific to the out-of-plane magnetization configuration. The insertion of a thin Pt layer at the Co/AFM interface, for example, increases the perpendicular exchange bias field.[9,11,12,16,17,20] Another interesting feature of $[Pt/Co]_n/Pt$/AFM multilayers is that it offers the opportunity to drastically alter the magnetization reversal process by slightly varying the Pt insertion layer thickness.[11,18,20] Consequently, it can be used to study the influence of spatial inhomogeneities on the magnetization reversal dynamics of exchange-coupled systems. For unbiased films, it is well known that structural and magnetic irregularities can alter the coercivity and magnetic domain structure.[26–30] Also, it has been shown that reversal asymmetries in exchange-biased systems with in-plane magnetization can be attributed to local variations in the magnetization angle and exchange bias direction.[31,32] A better understanding of the reversal dynamics in perpendicular exchange-biased layers is important for their potential application in field sensors and magnetic memories.[8,33,34]

In this paper, we quantitatively describe thermally activated magnetization reversal in exchanged-biased $[Pt/Co]_n/t$ Pt/IrMn multilayers with perpendicular magnetic anisotropy. The observed variations in the magnetization reversal process with Pt insertion layer thickness are explained within the framework of theoretical models that were originally developed for unbiased systems. Activation energy barriers and their dispersion are obtained from magnetization relaxation measurements. From our analysis, we conclude that a very high nucleation density for $t=0.1$ nm is predominantly due to a lateral variation of the interface exchange coupling energy and that reversal asymmetries result from an angular dispersion of the anisotropy axis and exchange bias direction.

This paper is organized as follows. In Sec. II, the fabrication of the $[Pt/Co]_n/Pt/IrMn$ multilayers and the experimental techniques that were used to characterize their magnetic properties are described. Theoretical models on thermally activated magnetization reversal are introduced in Sec. III. Section IV summarizes the experimental data and discusses the influence of local variations of the magnetization direction, the magnetic anisotropy energy, and the exchange coupling strength. Finally, the work is concluded in Sec. V.

II. EXPERIMENT

The $[2\ \text{nm Pt}/0.5\ \text{nm Co}]_3/t\ \text{nm Pt}/10\ \text{nm IrMn}/2\ \text{nm Pt}$ multilayers were grown onto 500 nm thick SiO_2 films by dc magnetron sputtering at room temperature. Although no perpendicular field was applied during deposition, the stray field from the magnetron guns (≈ 2.5 mT) was large enough to homogeneously magnetize the Co/Pt multilayers. Hence, the subsequent deposition of an IrMn film on top of these single-domain films established one unique perpendicular exchange bias direction. After deposition, the multilayers

were characterized by magneto-optical Kerr effect (MOKE) microscopy[35] and magnetometry.[36]

The Kerr system for real-time observations of the magnetic domain structure consisted of a microscope with a charge-coupled device camera, a frame grabber, and a source of magnetic field, which were all controlled by a computer.[35] The spatial resolution of the system was about 1 μm. The real-time part of the image processing software performed background subtraction, histogram equalization, and stored 20 s of the most recently acquired images. The offline part of the image processing software provided dynamic characterization of domain structures and was especially configured for precise measurements of magnetization relaxation curves and domain wall velocities. An electromagnet or Helmholtz coil in combination with a bipolar power supply generated the applied magnetic field. The power supply was driven by a 16 bit microprocessor providing a minimal field variation of $\Delta H=0.005$ mT.

The Kerr magnetometer[36] consisted of a differential amplifier enabling measurements up to a frequency of 1 kHz. The diode laser beam with a wavelength of 633 nm was polarized by a Glan-Thompson prism and subsequently reflected from the sample surface. A Wollaston prism split the reflected beam into two linearly polarized beams with mutually orthogonal planes. These beams were focused onto two photodiodes. The sum and difference of the photodiode signals were differentially amplified and subsequently measured by a computer with a high-resolution (16 bit) and rapid (200 kHz) analog-to-digital converter.

III. THEORY

Narrow Bloch walls separate magnetic domains in thin films with strong perpendicular anisotropy. The surface stray field energy of these walls is relatively small and can therefore be regarded as a second order term with respect to the uniaxial anisotropy energy of the FM film.[37] In the case of ultrathin cobalt layers, the width of a domain wall is in the nanometer range,[38] which is relatively small compared to the initial size of a magnetic domain. Under these conditions, the energy density of a magnetic domain in an exchange-biased system with perpendicular magnetic anisotropy can be approximated as

$$E(\theta) = -K_U \cos^2\theta - \mu_0 M_S H \cos(\theta - \phi) - \frac{\varepsilon_{\text{int}}}{t_{\text{Co}}} \cos\theta. \quad (1)$$

Here, θ is the angle of the film magnetization M_S with respect to the film normal, ϕ is the angle between the film normal and the axis of the applied magnetic field H, K_U is the perpendicular uniaxial anisotropy energy density, ε_{int} is the interface exchange coupling energy per unit area, and t_{Co} is the total Co layer thickness. Switching between the two perpendicular magnetization states, i.e., from $\theta=0°$ to $\theta=180°$ or vice versa, is hindered by an activation energy barrier $W(H)$, which for the forward (F) and backward (B) branches of the hysteresis loop is given by

$$W_F(H) = W_F + \mu_0 M_S H V_{BF}, \quad (2a)$$

$$W_B(H) = W_B - \mu_0 M_S H V_{BB}. \quad (2b)$$

Here, reversal in the forward direction is defined as a switch against the exchange bias direction, W is the activation energy barrier in zero applied magnetic field, and V_B equals the magnetization volume that reverses during a single activation event or the so-called Barkhausen volume. In the absence of thermally activated reversal events, the reversal process is completed only when H equals or exceeds a critical switching field H_S, for which $W(H=H_S)=0$. Magnetization reversal in Co/Pt multilayers, however, is thermally activated and as a result, the magnetization switches from a metastable state well below the critical switching field H_S and the switching probability is proportional to $\exp[-W(H)/k_BT]$.

Magnetization relaxation curves are a powerful tool for studying thermally activated reversal. The shape of $M(t)$ curves can be fitted by the Fatuzzo-Labrune model.[39,40] The main assumptions in this model are a random nucleation of cylindrical domains at a rate R and subsequent domain growth with a radial velocity v. The competition between the domain wall propagation and domain nucleation is expressed by a reversal parameter $k=v/r_cR$, where r_c is the initial domain radius. The fractional area of magnetization $B(t)$ not yet reversed in time, defined as $B(t)=(M(t)+M_S)/2M_S$, is given by

$$B(t) = \exp\{-2k^2[1-(Rt+k^{-1}) + 0.5(Rt+k^{-1})^2 - e^{-Rt}(1-k^{-1}) - 0.5k^{-2}(1-Rt)]\}. \quad (3)$$

If nucleation is the predominant reversal mechanism, k is very small ($k \ll 1$) and Eq. (3) simplifies to

$$B(t) = \exp(-Rt). \quad (4)$$

If, on the other hand, the magnetization switches by domain wall propagation, $k \gg 100$ and

$$B(t) = \exp\left(-\frac{k^2R^3t^3}{3}\right). \quad (5)$$

Both reversal processes are thermally activated and depend exponentially on the activation energy barrier

$$R = R_0 \exp[-W(H)/k_BT], \quad (6)$$

$$v = v_0 \exp[-W(H)/k_BT]. \quad (7)$$

By fitting magnetization relaxation curves, it is possible to determine the parameter k and hence the predominant reversal mechanism. Also, one can extract the time needed to reverse half of the film magnetization, t_{50}, which also depends exponentially on $W(H)$ following an Arrhenius law. According to Eq. (2), this dependence can be rewritten as

$$t_{50F} = t_0 \exp[(W_F + \mu_0 M_S H V_{BF})/k_BT], \quad (8a)$$

$$t_{50B} = t_0 \exp[(W_B - \mu_0 M_S H V_{BB})/k_BT]. \quad (8b)$$

The Barkhausen volume can be obtained from fits to $\ln(t_{50})$ vs H, $\ln(R)$ vs H, and $\ln(v)$ vs H plots. Additionally, the critical switching fields H_{SF} and H_{SB} for thermally activated reversal, defined as the fields for which $W(H)=0$, thus

$t_{50}/t_0=1$, can be determined from Eqs. (8a) and (8b). These fields can be used to extract the initial activation energy barrier for the forward branch of the hysteresis loop,

$$W_F = -\mu_0 M_S H_{SF} V_{BF}, \tag{9a}$$

as well as for the backward branch,

$$W_B = \mu_0 M_S H_{SB} V_{BB}. \tag{9b}$$

While Eqs. (1)–(9) can be used to determine important parameters such as the average activation energy barriers, the Barkhausen volume, and k, they do not properly explain the origin of contrasting magnetization reversal dynamics and switching asymmetries. To understand these effects, one needs to explicitly take into account the dispersion of the activation energy barrier, σ_W. Local variations in, for example, the magnetization direction, the magnetic anisotropy energy, and the exchange coupling strength determine the magnetic domain structure during reversal. Dispersions in the uniaxial anisotropy energy density (σ_{Ku}), interface exchange coupling energy density ($\sigma_{\varepsilon_{\text{int}}}$), and the anisotropy axis and exchange bias direction (σ_θ) can be incorporated into Eq. (1) as

$$E(\theta) = -(K_U \pm \sigma_{Ku})\cos^2(\theta \pm \sigma_\theta) - \mu_0 M_S H \cos(\theta - \phi) - \frac{(\varepsilon_{\text{int}} \pm \sigma_{\varepsilon\ \text{int}})}{t_{\text{Co}}} \cos(\theta \pm \sigma_\theta). \tag{10}$$

If the dispersion of the activation energy barrier is small, the nucleation of an inverse domain will trigger the reversal of neighboring spins leading to a fast domain wall motion. On the other hand, large σ_W will favor many isolated nucleation events. In this case, the lateral variation of the activation energy barrier is large and the domain wall motion is hampered.

Magnetization relaxation measurements can also be used to estimate the average dispersion of the activation energy barrier. If one assumes a square distribution of energy barriers and plots the fractional area of magnetization $B(t)$ that has not yet reversed in time as a function of $\ln(t)$, the maximum slope is inversely proportional to σ_W,[41]

$$\frac{dB}{d\ln(t)} = -\frac{k_B T}{2\sigma_W}. \tag{11}$$

For the two extreme cases, the Fatuzzo-Labrune model predicts

$$B(t) = \exp(-Rt) \Rightarrow -\left.\frac{dB}{d\ln(t)}\right|_{\max} = \frac{1}{e} \tag{12}$$

when the magnetization reverses by domain nucleation and

$$B(t) = \exp\left(-\frac{k^2 R^3 t^3}{3}\right) \Rightarrow -\left.\frac{dB}{d\ln(t)}\right|_{\max} = \frac{3}{e} \tag{13}$$

for switching by domain wall motion.

IV. RESULTS

Figure 1 shows magnetization relaxation curves for a $[2\ \text{nm Pt}/0.5\ \text{nm Co}]_3/10\ \text{nm IrMn}$ multilayer at different applied magnetic fields. The shape of the curves for (a) forward and (b) backward reversals is dissimilar, reflecting an asymmetry in the reversal process. Fitting the experimental data with Eq. (3) gives $k=2.6$ (forward) and $k=80$ (backward), which indicates that domain nucleation is more significant when the magnetization reverses against the exchange bias direction. From these curves, the time necessary to reverse half of the film magnetization t_{50} can be determined and its dependence on applied field is plotted in Fig. 2. Two reversal regimes can be distinguished. At relatively small field, magnetization reversal is thermally activated and t_{50} follows the Arrhenius law of Eq. (8). At larger field, however, switching becomes very fast and the data points start to deviate from the fit. In this regime, domain motion changes from a thermally activated mode to a viscous wall motion mode where domain nucleation becomes an increasingly more important reversal mechanism. Viscous wall motion was introduced in a reversal model by Raquet *et al.* to account for nonthermally activated processes in the high dynamical regime.[42] Recently, we demonstrated that the exchange bias field also depends on the reversal mode.[43] The exchange bias field of our perpendicularly biased samples was found to decrease at high field sweep rates where domain nucleation becomes the predominant reversal mecha-

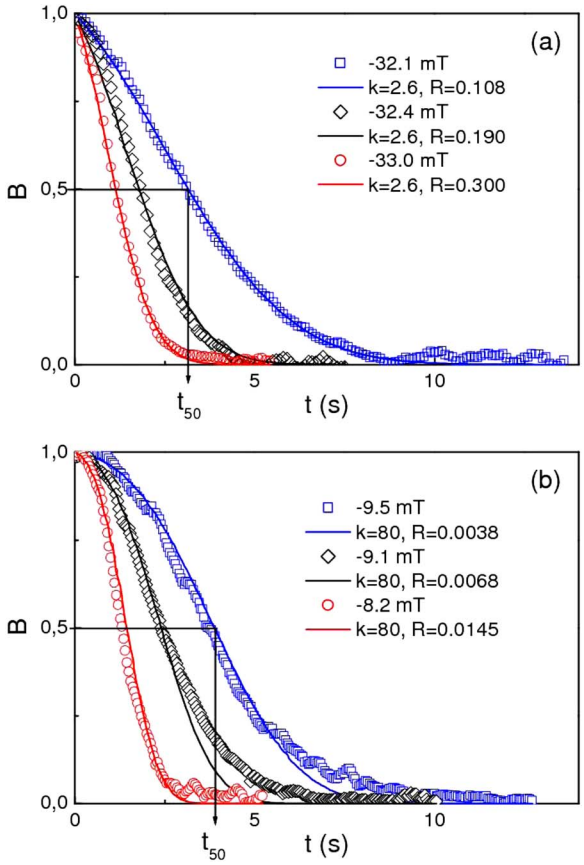

FIG. 1. (Color online) Magnetization relaxation curves of a $[2\ \text{nm Pt}/0.5\ \text{nm Co}]_3/10\ \text{nm IrMn}$ multilayer at different applied magnetic fields. The curves were obtained by an abrupt change of the applied magnetic field from saturation to just below (a) the forward and (b) the backward switching fields. The lines indicate fits to the data using Eq. (3) (Fatuzzo-Labrunne model).

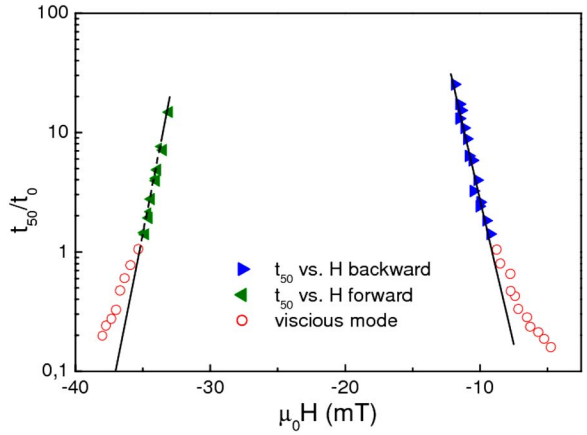

FIG. 2. (Color online) Time necessary to reverse half of the film magnetization, t_{50}, as a function of applied magnetic field for a $[2\ \text{nm Pt}/0.5\ \text{nm Co}]_3/10\ \text{nm IrMn}$ multilayer. The solid symbols represent thermally activated reversal and can be fitted by the Arrhenius law of Eq. (8). The transition to a viscous reversal mode is indicated by open symbols. The critical switching fields for reversal in the forward and backward directions are $\mu_0 H_{SF} = -35$ mT and $\mu_0 H_{SB} = -9$ mT, respectively.

nism. In Fig. 2, the critical switching fields ($t_{50}/t_0 = 1$) are −35 and −9 mT for forward and backward reversals, respectively. Similar $\ln(t_{50})$ vs H curves were measured on exchange-biased Co/Pt multilayers with different Pt insertion layer thicknesses. The critical switching fields of all films are summarized in Fig. 4(a).

Figure 3 shows the nucleation rate R and domain wall velocity v for a $[2\ \text{nm Pt}/0.5\ \text{nm Co}]_3/10\ \text{nm}$ IrMn multilayer as a function of applied magnetic field, as determined from magnetization relaxation curves (Fig. 1) and real-time Kerr microscopy movies. Fitting the data with Eqs. (6) and (7) and using $M_S = 1.42 \times 10^6$ A/m give Barkhausen volumes of $V_{BF} = (3.5 \pm 0.3) 10^{-24}$ m^3 and $V_{BB} = (3.2 \pm 0.3) 10^{-24}$ m^3 for the forward and backward branches of the hysteresis loop, respectively.[44] Alternatively, the Barkhausen volume can be estimated from $\ln(t_{50})$ vs H curves (Fig. 2). Fitting those data with Eq. (8) gives $V_{BF} = (3.9 \pm 0.2) 10^{-24}$ m^3 and $V_{BB} = (3.3 \pm 0.25) 10^{-24}$ m^3. Average values of V_B are plotted in Fig. 4(b) as a function of the Pt insertion layer thickness t. The Barkhausen volume is largest for $t = 0.1$ nm, a sample in which the magnetization reverses predominantly by domain nucleation (see below). In addition, the reversal volumes are slightly larger for switching in the forward branch of the hysteresis loop when t is small. This contrasts results by Garcia *et al.* on $[\text{Pt}/\text{Co}]_n/\text{FeMn}$ multilayers, indicating a smaller Barkhausen volume for reversal in the forward direction.[45] Dissimilar values of V_{BF} and V_{BB} are another manifestation of reversal asymmetry in exchange-biased Co/Pt multilayers.

Using the switching fields from the $\ln(t_{50})$ vs $\mu_0 H$ plots and the average Barkhausen volumes, we calculated the initial activation energy barriers W with Eq. (9a) and (9b). The results for $[2\ \text{nm Pt}/0.5\ \text{nm Co}]_3/t\ \text{nm Pt}/10\ \text{nm IrMn}$ multilayers with different t are summarized in Fig. 4(c). The difference between the initial activation energy barrier for

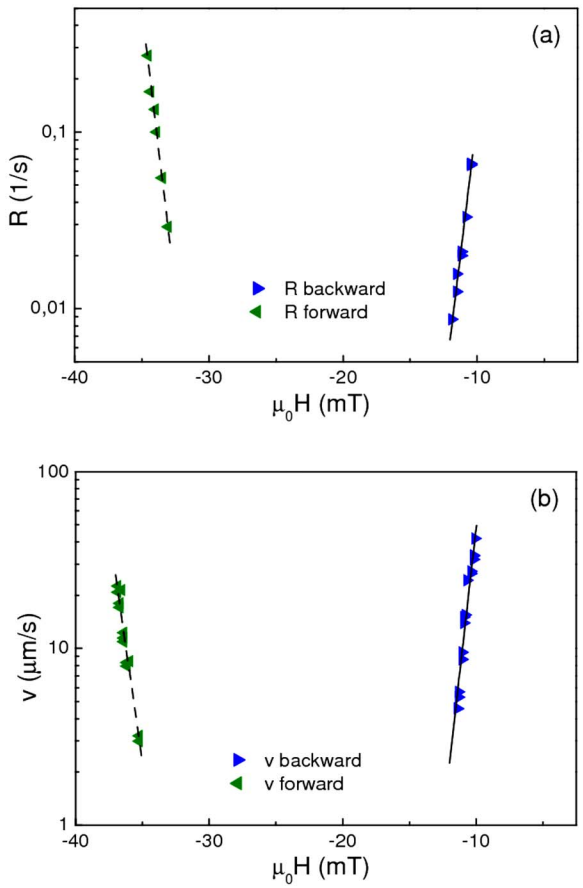

FIG. 3. (Color online) (a) Domain nucleation rate R and (b) domain wall velocity $[2\ \text{nm Pt}/0.5\ \text{nm Co}]_3/10\ \text{nm}$ IrMn multilayer.

forward and backward reversals is largest for $t = 0.1$ nm. For thicker Pt insertion layers, the activation barriers converge at about 0.17 eV, which is similar to that of the unbiased Co/Pt multilayer. The Pt insertion layer thickness dependence of the exchange coupling energy, $W_{EB} = (W_F - W_B)/2$, is plotted in Fig. 4(d). The exchange coupling energy for $t = 0$ nm, i.e., for a direct contact between the outermost Co film and the IrMn layer, is 0.72 eV. This corresponds to an interface coupling energy per unit area of $\varepsilon_{\text{int}} = (W_F/2V_{FB} - W_B/2V_{BB}) t_{\text{Co}} = 4.7 \times 10^{-5}$ J/m^2, which is smaller than the coupling energy of an in-plane 5 nm Co/10 nm IrMn bilayer grown under the same conditions.[46] An angular dispersion of the magnetization direction (σ_θ) is the main reason for the reduction of the exchange coupling energy in Co/Pt multilayers with perpendicular magnetic anisotropy. As the Co/IrMn interface favors in-plane magnetization,[16] the Co moment tends to tilt away from the film normal, thereby reducing the perpendicular spin projection and hence the exchange coupling energy. The insertion of a thin Pt layer at the Co/IrMn interface increases the perpendicular anisotropy[9] and hence reduces σ_θ. As a result, the exchange coupling energy increases to 1.04 eV for $t = 0.1$ nm, which corresponds to $\varepsilon_{\text{int}} = 5.7 \times 10^{-5}$ J/m^2. For thicker Pt insertion layers, however, the Co and IrMn layers become increasingly decoupled and this reduces the exchange bias energy, as illustrated by the data of Fig. 4(d).

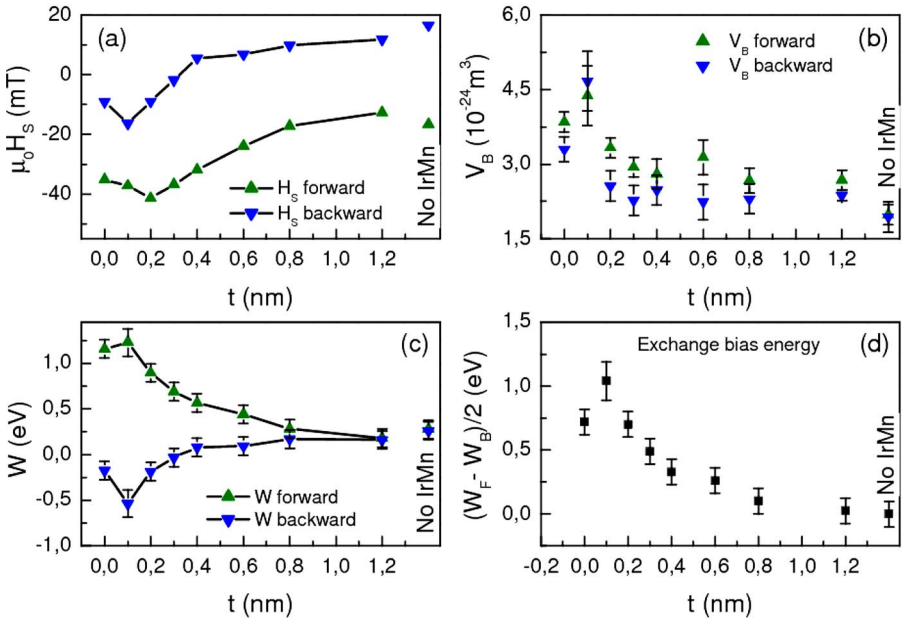

FIG. 4. (Color online) (a) Critical switching fields, (b) Barkhausen volumes, (c) initial activation energy barriers, and (d) exchange coupling energy of $[2\ \text{nm Pt}/0.5\ \text{nm Co}]_3/t$ Pt/10 nm IrMn multilayers as a function of Pt insertion layer thickness t.

Figure 5 shows magnetization relaxation curves of $[2\ \text{nm Pt}/0.5\ \text{nm Co}]_3/t$ nm Pt/10 nm IrMn multilayers with $t=0$ nm, $t=0.1$ nm, and $t=1.2$ nm together with corresponding Kerr microscopy images of the reversal process. Here, the magnetization not yet reversed in time, $B(t)$, is plotted versus $\ln(t)$ so that the maximum slope equals $-k_BT/2\sigma_W$ [Eq. (11)]. For $t=0$ nm, the dispersion of the activation energy barrier, σ_W, is different for the two branches of the hysteresis loop. The largest value is obtained when the film magnetization is switched against the exchange bias direction. This indicates that domain nucleation plays a larger role during forward reversal. This is confirmed by the MOKE microscopy images of Figs. 5(a) and 5(b) and is also apparent from fits to the relaxation curves of Fig. 1 (the parameter $k=v/r_cR$ is smaller for reversal in the forward direction). Asymmetric magnetization reversal is a general feature of the $[2\ \text{nm Pt}/0.5\ \text{nm Co}]_3/t$ nm Pt/10 nm IrMn multilayers with $t\leqslant 0.8$ nm. One exception is the sample with $t=0.1$ nm. For this very thin Pt insertion layer, the domain structure during reversal is considerably different, as illustrated by the MOKE microscopy images of Fig. 5(c). In this case, many small domains nucleate and the domain wall motion is relatively slow. This is confirmed by the fit to the magnetization relaxation curve of Fig. 5(c) yielding $\sigma_W=0.038\pm0.003$ eV, whose error margin is within the maximum dispersion value of $-k_BTe/2(=0.0352\ \text{eV})$ given by the Fatuzzo-Labrune model for pure domain nucleation ($k\rightarrow 0$). In addition, magnetic switching in the Co/Pt multilayer with $t=0.1$ nm is much more symmetric than for the other exchange-biased samples. Finally, Fig. 5(d) shows a magnetization relaxation curve and corresponding MOKE microscopy images for $t=1.2$ nm. For this sample, the Pt insertion layer magnetically decouples the Co/Pt multilayer and the IrMn film, leading to zero bias and symmetric reversal by fast domain wall motion.

The dispersions of the activation energy barrier are summarized in Fig. 6. The main results, a significantly enhanced dispersion for $t=0.1$ nm and reversal asymmetry for $t\leqslant 0.8$ nm, are evident. To interpret the large variations in the magnetization reversal dynamics with increasing Pt insertion layer thickness, dispersions in the uniaxial anisotropy energy density (σ_{Ku}), interface exchange coupling energy ($\sigma_{\varepsilon_{\text{int}}}$), and magnetization angle (σ_θ) need to be taken into account. For Co/Pt multilayers without IrMn, the exchange bias term in Eq. (10) can be omitted and the dispersion of the activation energy barrier $\sigma_W=0.004$ eV is easily reproduced by an 11% variation of the perpendicular anisotropy energy density K_U. This relatively small dispersion of the anisotropy energy could be explained by lateral fluctuations in the Co layer thickness, interface roughness, or other structural defects.

A similar analysis of the Co/Pt multilayer with $t=0.1$ nm shows that the large dispersion of $\sigma_W=0.038$ eV can be simulated when one assumes that the anisotropy energy K_U varies by about 26%. This value for σ_{Ku} is, however, too large to be physically feasible if one compares it to the anisotropy dispersion of unbiased Co/Pt multilayers as it would constitute a 136% increase. Although replacing one of the six Co/Pt interfaces by a Co/IrMn interface does reduce the magnetic anisotropy of the multilayer stack, it has been found to be a rather modest reduction of about −30%.[16] Alternatively, a lateral fluctuation of the interface exchange coupling energy, ε_{int}, can also enhance the dispersion of the activation energy barrier. In this case, a ratio of $\sigma_{\varepsilon_{\text{int}}}/\varepsilon_{\text{int}}$ of 10% is sufficient to reproduce $\sigma_W=0.038$ eV. Such a variation of the exchange coupling energy is comprehensible for $t=0.1$ nm, where the Pt insertion layer is discontinuous and thin Pt islands decorate the Co/IrMn interface. The areas where the outermost Co film is in direct contact with the IrMn layer experience an exchange coupling that is similar to that of a $[\text{Pt}/\text{Co}]_3$/IrMn multilayer without Pt insertion layer. The exchange coupling in areas with Pt at the Co/IrMn interface, on the other hand, is enhanced due to an improved Co spin alignment along the film normal. The effect of a discontinuous Pt layer at the Co/IrMn interface is therefore twofold: (1) it increases the average exchange bias field and (2) it enhances the dispersion of the activation energy barrier

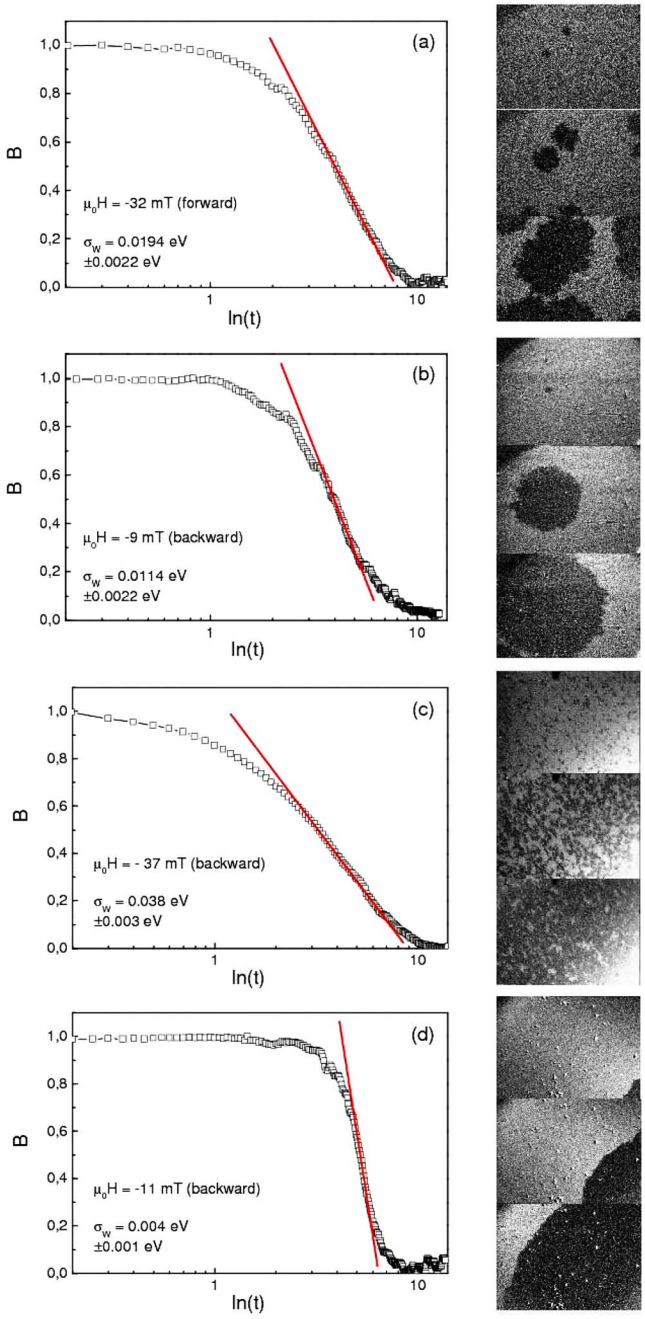

FIG. 5. (Color online) Magnetization relaxation curves as a function of $\ln(t)$ and MOKE microscopy images of $[2\ \text{nm Pt}/0.5\ \text{nm Co}]_3/t$ Pt/10 nm IrMn multilayers with [(a) and (b)] $t=0$ nm, (c) $t=0.1$ nm, and (d) $t=1.2$ nm. The lines indicate the maximum slope which is given by $-k_BT/2\sigma_W$. The image area is $200\times250\ \mu\text{m}^2$.

leading to magnetization reversal by domain nucleation rather than domain wall propagation.

Interestingly, the different values of σ_W for reversal into the forward and backward directions ($t=0$ nm and $t=0.2-0.8$ nm) can neither be reproduced by a dispersion of K_U nor by a variation of ε_{int}. Instead, only lateral fluctuations of the anisotropy axis and exchange bias direction can account for the reversal asymmetry in these samples. This is illustrated by the angular dependence of the activation

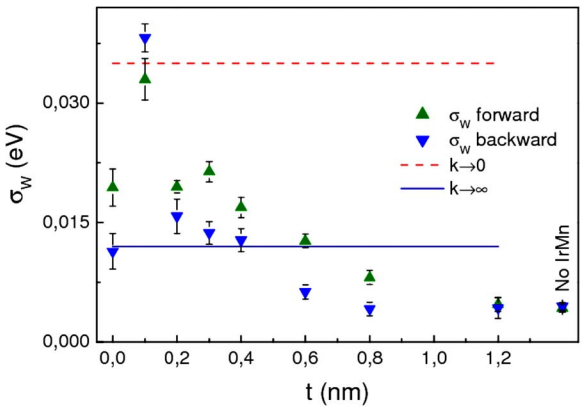

FIG. 6. (Color online) Dispersion of the activation energy barrier for forward and backward reversals in $[2\ \text{nm Pt}/0.5\ \text{nm Co}]_3/t$ Pt/10 nm IrMn multilayers as a function of Pt insertion layer thickness t. The dashed line indicates the Fatuzzo-Labrune dispersion limit for reversal by domain nucleation and the solid line indicates the dispersion limit for magnetic switching by domain wall propagation.

energy in Fig. 7. In these model calculations, it is assumed that $K_U=1.2\times10^4\ \text{J/m}^3$, $\varepsilon_{\text{int}}=4.7\times10^{-5}\ \text{J/m}^2$, $V_B=3.67\times10^{-24}\ \text{m}^3$, and σ_θ is varied continuously from $\sigma_\theta=-3°$ to $\sigma_\theta=3°$ and back in the energy versus angle plots.[47] At an applied field of −34.3 mT, i.e., a relatively large negative field that resembles the forward switching field, the calculations yield $\sigma_W=0.0194$ eV. This dispersion of the activation energy barrier is considerably larger than $\sigma_W=0.0104$ eV, which is obtained at a small negative applied field of −9.7 mT where the magnetization reverses into the backward direction. The experimental results on reversal asymmetry (Fig. 6) are therefore qualitatively explained by taking into account a small variation of the magnetization direction around the film normal. Moreover, the influence of spatial variations in σ_θ on the magnetization reversal mechanism is clearly illustrated by Fig. 7. The rather homogeneous energy landscape near the critical field for backward reversal [Fig. 7(b)] promotes a quickly propagating spin switching sequence from $\theta=-180°$ to $\theta=0°$ after the nucleation of an inverse domain. In the forward branch [Fig. 7(a)], on the other hand, the energy barrier dispersion σ_W is considerably larger. This leads to a slower domain wall motion and an enhanced domain nucleation in agreement with the magnetization relaxation measurements and MOKE microscopy images. Finally, we note that asymmetric magnetization reversal can also be obtained when one assumes a misalignment between the exchange bias direction and the axis of the applied magnetic field, i.e., $\phi\neq0$.[48,49] However, whereas lateral variations of the anisotropy axis and the exchange bias direction will always yield larger energy barrier dispersions for forward reversal, the polarity of the asymmetry would change with the sign of ϕ. The latter does not occur in our experiments from which we conclude that the applied magnetic field was properly aligned along the film normal.

V. CONCLUSIONS

The exchange coupling energy and magnetization reversal dynamics in $[2\ \text{nm Pt}/0.5\ \text{nm Co}]_3/t$ nm Pt/10 nm IrMn

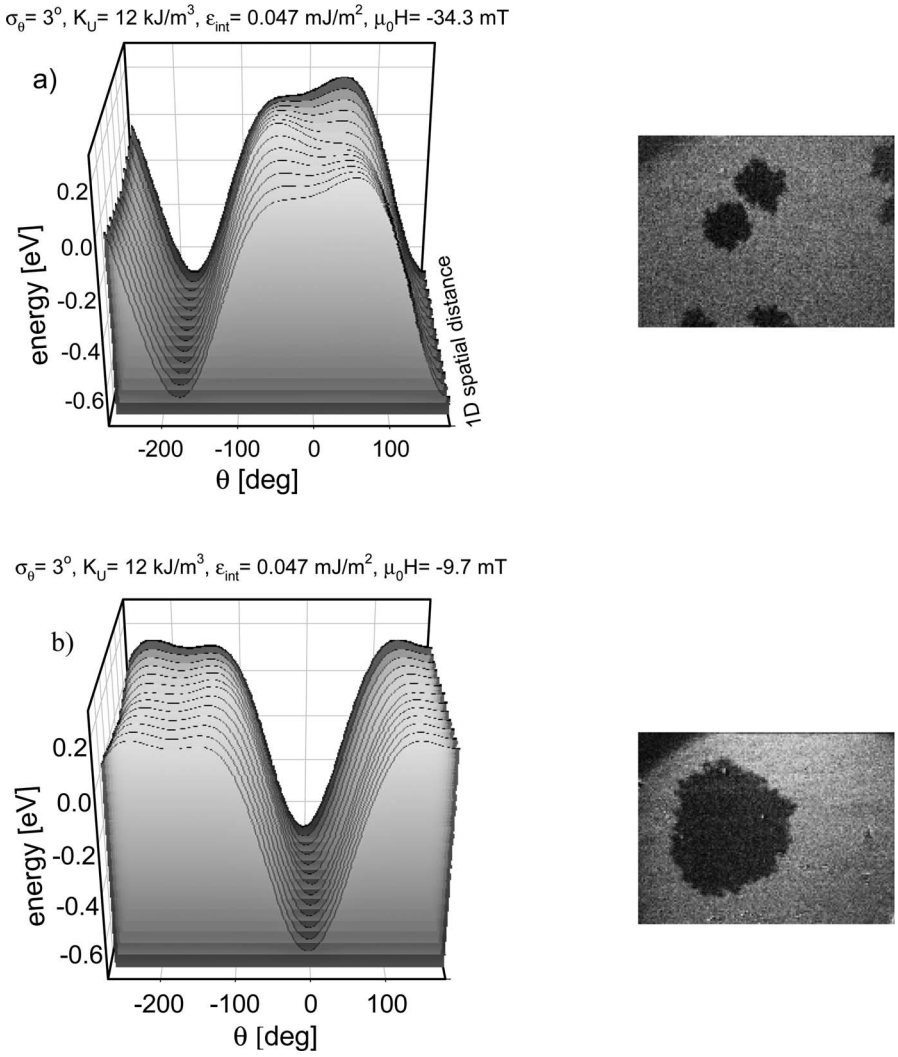

FIG. 7. Model calculations of the magnetic energy as a function of magnetization angle θ near the switching fields for (a) forward and (b) backward reversals. The MOKE images show the domain structure during magnetic switching in the two branches of the hysteresis loop for a $[2\ \text{nm Pt}/0.5\ \text{nm Co}]_3/10\ \text{nm}$ IrMn multilayer. The image area is $200\times250\ \mu\text{m}^2$.

multilayers depend strongly on the Pt insertion layer thickness t. The exchange coupling energy is largest for $t=0.1$ nm ($W_{EB}=1.04$ eV) due to an improved perpendicular spin alignment in the outermost Co film. A further increase of t decreases the exchange coupling energy monotonically and for $t=1.2$ nm the Co film and IrMn layer become entirely decoupled. Two types of magnetization reversal dynamics do occur in exchange-biased Co/Pt multilayers. For $t=0$ nm and $t=0.2-0.8$ nm, magnetization reversal proceeds by domain nucleation followed by a fast domain wall motion. In addition, the reversal process is asymmetric. This asymmetry is predominantly due to a lateral fluctuation of the anisotropy axis and exchange bias direction leading to a larger dispersion of the activation energy barrier at higher switching field (i.e., forward reversal branch). As a result, more domains nucleate when the magnetization reverses against the exchange bias direction. For $t=0.1$ nm, magnetization reversal proceeds by domain nucleation. The large dispersion of the activation energy barrier in this sample is predominantly caused by lateral variations in the interface exchange coupling energy. These variations are a result of the discontinuous nature of the Pt layer at the Co/IrMn interface where areas with Pt experience a larger exchange coupling than areas where the outermost Co film is directly contacted by the IrMn layer.

ACKNOWLEDGMENTS

This work was supported by the Polish Ministry of Science and higher Education as a part of projects for years 2006–2007 and by the Science Foundation Ireland.

*czapkiew@agh.edu.pl
†Present address: VTT Micro and Nanoelectronics, P.O. Box 1000, FI-02044 VTT, Finland; sebastiaan.van.dijken@vtt.fi

[1] W. H. Meiklejohn and C. P. Bean, Phys. Rev. **102**, 1413 (1956).
[2] S. Maat, K. Takano, S. S. P. Parkin, and E. E. Fullerton, Phys. Rev. Lett. **87**, 087202 (2001).
[3] O. Hellwig, S. Maat, J. B. Kortright, and E. E. Fullerton, Phys. Rev. B **65**, 144418 (2002).

[4] T. L. Kirk, O. Hellwig, and E. E. Fullerton, Phys. Rev. B **65**, 224426 (2002).
[5] P. Kappenberger, S. Martin, Y. Pellmont, H. J. Hug, J. B. Kortright, O. Hellwig, and E. E. Fullerton, Phys. Rev. Lett. **91**, 267202 (2003).
[6] F. Garcia, G. Casali, S. Auffret, B. Rodmacq, and B. Dieny, J. Appl. Phys. **91**, 6905 (2002).
[7] J. Sort, B. Rodmacq, S. Auffret, and B. Dieny, Appl. Phys. Lett. **83**, 1800 (2003).
[8] F. Garcia, F. Fettar, S. Auffret, B. Rodmacq, and B. Dieny, J. Appl. Phys. **93**, 8397 (2003).
[9] F. Garcia, J. Sort, B. Rodmacq, S. Auffret, and B. Dieny, Appl. Phys. Lett. **83**, 3537 (2003).
[10] C. H. Marrows, Phys. Rev. B **68**, 012405 (2003).
[11] F. Romanens, S. Pizzini, J. Sort, F. Garcia, J. Camarero, F. Yokaichiya, Y. Pennec, J. Vogel, and B. Dieny, Eur. Phys. J. B **45**, 185 (2005).
[12] J. Sort, F. Garcia, B. Rodmacq, S. Auffret, and B. Dieny, J. Magn. Magn. Mater. **272-276**, 355 (2004).
[13] X. Ji, H. Ju, D. E. McCready, and K. M. Krishnan, J. Appl. Phys. **98**, 116101 (2005).
[14] X. Ji and K. M. Krishnan, J. Appl. Phys. **99**, 08C105 (2006).
[15] S. van Dijken, J. Moritz, and J. M. D. Coey, J. Appl. Phys. **97**, 063907 (2005).
[16] S. van Dijken, M. Besnier, J. Moritz, and J. M. D. Coey, J. Appl. Phys. **97**, 10K114 (2005).
[17] J. Sort, V. Baltz, F. Garcia, B. Rodmacq, and B. Dieny, Phys. Rev. B **71**, 054411 (2005).
[18] J. Sort, B. Dieny, and J. Nogues, Phys. Rev. B **72**, 104412 (2005).
[19] F. Romanens, S. Pizzini, F. Yokaichiya, M. Bonfim, Y. Pennec, J. Camarero, J. Vogel, J. Sort, F. Garcia, B. Rodmaq, and B. Dieny, Phys. Rev. B **72**, 134410 (2005).
[20] M. Czapkiewicz, S. van Dijken, T. Stobiecki, R. Rak, M. Zoladz, and P. Mietniowski, Phys. Status Solidi C **3**, 48 (2006).
[21] S. van Dijken, M. Czapkiewicz, M. Zoladz, and T. Stobiecki, Phys. Status Solidi B **243**, 169 (2006).
[22] B. Kagerer, Ch. Binek, and W. Kleemann, J. Magn. Magn. Mater. **217**, 139 (2000).
[23] Ch. Binek, P. Borisov, Xi Chen, A. Hochstrat, S. Sahoo, and W. Kleemann, Eur. Phys. J. B **45**, 197 (2005).
[24] S. van Dijken, M. Crofton, and J. M. D. Coey, J. Magn. Magn. Mater. **290-291**, 1290 (2005).
[25] H. Xi, T. F. Ambrose, T. J. Klemmer, R. van de Veerdonk, J. K. Howard, and R. M. White, Phys. Rev. B **72**, 024447 (2005).
[26] H.-P. D. Shieh and M. H. Kryder, IEEE Trans. Magn. **24**, 2464 (1988).
[27] J. Pommier, P. Meyer, G. Pénissard, J. Ferré, P. Bruno, and D. Renard, Phys. Rev. Lett. **65**, 2054 (1990).
[28] M. Speckmann, H. P. Oepen, and H. Ibach, Phys. Rev. Lett. **75**, 2035 (1995).
[29] P. Haibach, M. Huth, and H. Adrian, Phys. Rev. Lett. **84**, 1312 (2000).
[30] S. B. Choe and S. C. Shin, Phys. Rev. B **62**, 8646 (2000).
[31] C. Hou, J. Chen, M. T. Kief, Z. Gao, S. Mao, and T. Pokhil, Appl. Phys. Lett. **78**, 237 (2001).
[32] J. McCord, R. Schäfer, R. Mattheis, and K.-U. Barholz, J. Appl. Phys. **93**, 5491 (2003).
[33] S. van Dijken and J. M. D. Coey, Appl. Phys. Lett. **87**, 022504 (2005).
[34] S. van Dijken, M. Crofton, M. Czapkiewicz, M. Zoladz, and T. Stobiecki, J. Appl. Phys. **99**, 083901 (2006).
[35] M. Zoladz, S. Knappmann, M. Otto, K. Röll, and T. Stobiecki, Phys. Status Solidi A **189**, 791 (2002).
[36] J. Wrona, T. Stobiecki, R. Rak, M. Czapkiewicz, F. Stobiecki, L. Uba, J. Korecki, T. Slezak, J. Wilgocka-Slezak, and M. Rots, Phys. Status Solidi A **196**, 161 (2003).
[37] A. Hubert and R. Schafer, *Magnetic Domains: The Analysis of Magnetic Microstructures* (Springer-Verlag, Berlin, 1998), pp. 257 and 306.
[38] U. Nowak, J. Heimel, T. Kleinefeld, and D. Weller, Phys. Rev. B **56**, 8143 (1997).
[39] E. Fatuzzo, Phys. Rev. **127**, 1999 (1962).
[40] M. Labrune, S. Andrieu, F. Rio, and P. Bernstein, J. Magn. Magn. Mater. **80**, 211 (1989).
[41] P. Bruno, G. Bayreuther, P. Beauvillain, C. Chappert, G. Lugert, D. Renard, J. P. Renard, and J. Seiden, J. Appl. Phys. **68**, 5759 (1990).
[42] B. Raquet, R. Mamy, and J. C. Ousset, Phys. Rev. B **54**, 4128 (1996).
[43] G. Malinowski, S. van Dijken, M. Czapkiewicz, and T. Stobiecki, Appl. Phys. Lett. **90**, 082501 (2007).
[44] Here, we use $M_S=1.42\times10^6$ A/m, which represents the saturation magnetization of bulk Co. The actual saturation magnetization of Co/Pt multilayers is smaller. For $[2\text{ nm Pt}/0.5\text{ nm Co}]_3/t$ nm Pt/10 nm IrMn/2 nm Pt, we measured a value of 0.8×10^6 A/m. The use of this value will enhance the Barkhausen volumes by about 80%. The other experimentally determined properties such as the initial activation energy barriers (W_F and W_B) and exchange coupling energy (W_{EB}) do, however, not depend on the value that is used for M_S. For example, $W_F=-\mu_0 M_S V_{BF} H_{SF}$ [Eq. (9a)], where H_{SF} follows from $t_{50}/t_0=1$ in Fig. 2 and $-\mu_0 M_S V_{BF}$ corresponds to the slope of the graph in Fig. 2 times k_BT (or the slope of the graphs in Fig. 3 times k_BT).
[45] F. Garcia, J. Moritz, F. Ernult, S. Auffret, B. Rodmacq, B. Dieny, J. Camarero, Y. Pennec, S. Pizzini, and J. Vogel, IEEE Trans. Magn. **38**, 2730 (2002).
[46] M. Czapkiewicz, T. Stobiecki, R. Rak, M. Zoladz, and S. van Dijken, J. Magn. Magn. Mater. **316**, 151 (2007).
[47] In this analysis, the perpendicular anisotropy energy density is chosen so that the angular dependence of the activation energy plots illustrates the magnetization reversal near the experimentally measured switching fields. The actual magnetic anisotropy of exchange-biased Co/Pt multilayers is larger (see, for example, Refs. 15 and 16) but due to local anisotropy fluctuations and thermal activation, the magnetization switches from a metastable state below the average anisotropy field.
[48] B. Beckmann, U. Nowak, and K. D. Usadel, Phys. Rev. Lett. **91**, 187201 (2003).
[49] J. Camarero, J. Sort, A. Hoffmann, J. M. García-Martín, B. Dieny, R. Miranda, and J. Nogués, Phys. Rev. Lett. **95**, 057204 (2005).